Journal of Power Sources 255 (2014) 242–250

Contents lists available at ScienceDirect

Journal of Power Sources

journal homepage: www.elsevier.com/locate/jpowsour

Kinetics of oxygen reduction reaction on three different Pt surfaces of Pt/C catalyst analyzed by rotating ring-disk electrode in acidic solution

Lei Zhang, Hui Li, Jiujun Zhang*

National Research Council of Canada, Vancouver, BC, Canada

HIGHLIGHTS

- ORR on a Pt/C-based thin catalyst layer is studied using RRDE technique.
- A modified model for ORR constants is validated.
- Pure Pt surface has the best ORR activity compared to others (Pt–H and PtO_X/Pt).

ARTICLE INFO

Article history:
Received 7 October 2013
Received in revised form
7 January 2014
Accepted 8 January 2014
Available online 15 January 2014

Keywords:
Oxygen reduction reaction
Pt/C catalyst
Kinetic constants
Pt surface structure

ABSTRACT

The oxygen reduction reaction (ORR) on a Pt/C-based thin catalyst layer is studied using the rotating ring-disk electrode (RRDE) technique in an O_2-saturated acid solution. A modified model for obtaining the ORR constants in different electrode potential ranges is validated using the experimental disk and ring currents. The results calculated from the model and the Koutecky–Levich plots reveal that the ORR constants on three different Pt surfaces (Pt–H, Pt, and PtO_X/Pt) are significantly different, among which, pure Pt surface is found to have the best activity towards ORR. This model can also give a detailed formularization of the apparent ORR electron transfer number (n) and the percentage of H_2O_2 ($\%H_2O_2$) produced during the ORR process.

1. Introduction

With the progress of fuel cell technology, Pt-based catalysts for catalyzing the cathodic fuel cell oxygen reduction reaction (ORR) have been identified as the most practical catalysts at current state of technology [1]. In order to further improve Pt/C catalyst performance, a fundamental understanding of the catalyst's ORR activity through both experimental measurements and theoretical simulation is important and necessary in developing new catalysts, even though the behavior of ORR on Pt/C nanoparticle surfaces may be similar to that of a polycrystalline smooth Pt surface. In these efforts, the rotating ring-disk electrode (RRDE) technique has been recognized as the most powerful tool for the activity evaluation of ORR catalysts, and also the most commonly used technique in practice.

Using disk and ring currents collected by RRDE technique at different electrode rotation rates, the models developed by Bocris' group [2–4] have been used for data analysis to simulate all ORR-related reaction constants. Since then, the models have also been modified and validated by many other groups [5–11]. The general approaches to obtain the reaction constants are based on the steady-state mass balances of the O_2 consumed and H_2O_2 produced during the ORR process on both rotating disk and the ring electrodes. It seems that the emphasizes have been mainly given to the reaction mechanism aspects from which the reaction constants are derived, but less on the effect of electrode surface states at different potentials. In this paper, we have put our emphasis on the effect of Pt electrode surface states.

It is believed that the ORR activity of Pt-based catalysts is strongly dependent on the state(s) of the Pt surface. In different potential ranges, Pt has different surface structures such as: hydrogen-adsorbed Pt surface, pure Pt surface, and oxide covered Pt surface, where each structure should have a different ORR activity. In this paper, a typical Pt/C-based thin catalyst layer was fabricated on a rotating disk electrode and its' ORR activity was studied using the RRDE technique in an O_2-saturated acid solution. Based on a modified model similar to those in the literature, the ORR rate constants in the potential range of 0.05–0.85 V vs. RHE

* Corresponding author. Tel.: +1 604 221 3087.
E-mail address: Jiujun.zhang@nrc.gc.ca (J. Zhang).

0378-7753/$ – see front matter © 2014 Elsevier B.V. All rights reserved.
http://dx.doi.org/10.1016/j.jpowsour.2014.01.042

Nomenclature

$B_{O_2}(=0.201D_{O_2}^{2/3}\nu^{-1/6})$	diffusion constant of O_2 (cm $s^{-1/2}$)
$B_{H_2O_2}(=0.201D_{H_2O_2}^{2/3}\nu^{-1/6})$	diffusion constant of H_2O_2 (cm $s^{-1/2}$)
$C_{O_2}^o$	bulk solution concentration of O_2 (mol cm^{-3})
$C_{O_2}^s$	O_2 concentration near the electrode surface (mol cm^{-3})
$C_{H_2O_2}^o$	bulk solution concentration of H_2O_2 (mol cm^{-3})
$C_{H_2O_2}^s$	H_2O_2 concentration near the electrode surface (mol cm^{-3})
D_{O_2}	O_2 diffusion coefficient (1.9×10^{-5} cm^2 s^{-1})
$D_{H_2O_2}$	H_2O_2 diffusion coefficient (1.5×10^{-5} cm^2 s^{-1})
F	Faraday's constant (96487 C mol^{-1})
I_d	disk electrode current (mA)
I_{dl,O_2}	limiting current for ORR (mA)
I_{dl,H_2O_2}	limiting current for H_2O_2 production (mA)
I_{dl,O_2}^T	theoretical ORR limiting current (mA)
I_r	ring electrode current (mA)
I_k	kinetic current of ORR (mA)
k_i	rate constant of reaction (i) (cm s^{-1})
n	apparent electron number of ORR
N	ring electrode collection efficient (0.37)
r	radius of the rotating disk electrode (cm)
ν	kinematic viscosity of the electrolyte solution (cm^2 s^{-1})
ω	rotation rate of the disk electrode (RPM)
$\%H_2O_2$	percentage of H_2O_2 produced during ORR

were obtained on different Pt surface states, and were also validated using experimental disk and ring currents. In addition, this modified model could also give the detailed derivation to obtain the formulas for calculating the apparent ORR electron transfer number (n) and the percentage of H_2O_2 produced during the ORR process (% H_2O_2) at different ORR mechanisms, which have not been emphasized in the literature.

2. Experimental

2.1. Structure of the rotating ring-disk electrode (RRDE)

For RRDE measurements, a glassy carbon disk electrode with a geometric area of 0.25 cm^2 (Pine Instruments) was used as the working electrode on which a thin catalyst layer was coated. Surrounding this disk electrode, there was a Pt ring electrode. The collection efficiency, 0.37, of this RRDE electrode was calibrated using 0.01 M $K_4[Fe(CN)_6]$ + 0.5 M H_2SO_4 aqueous solution.

2.2. Preparation of the catalyst layer on the disk electrode

For the catalyst layer coating, a pre-polished and cleaned glassy carbon disk electrode surface was used as the substrate. A commercially available carbon supported Pt powder (Pt/C, 46.9 wt% Pt purchased from TKK) was used as the catalyst for catalyst ink preparation. In the catalyst ink preparation, the as-received Pt/C catalyst powder was dispersed in a solution consisting of 95% isopropanol (from Sigma–Aldrich), 5% DI water (18 MΩ cm from Millipore Milli-Q system) and 5% Nafion® ionomer (Alfa-Aesar) under ultrasonication for 30 min (note that the weight ratio of Nafion® to Pt/C in this catalyst ink was 1:21). In preparation of the catalyst layer, the catalyst ink was pipetted onto the glassy carbon disk surface with a Pt loading of 48 μg cm^{-2}. After drying in the air, this working electrode was transferred into the electrochemical cell for measurements.

2.3. Preparation of the electrolyte solution

The electrolyte solution used in this paper was 0.5 M H_2SO_4 aqueous solution, prepared using reagent grade sulfuric acid (Acros). For surface cyclic voltammograms, this solution was deaerated by purging with nitrogen (99.999%, Praxair) for 30 min before each measurement. For measuring catalyst ORR activity, this solution was saturated with oxygen (99.999%, Praxair) through constant bubbling for 30 min before each measurement and kept bubbling during the measurements.

2.4. Electrochemical measurements

A conventional three-electrode electrochemical cell was used for all electrochemical measurements, which contained a catalyst coated RRDE electrode as working electrode, a platinum black coated wire as counter electrode, and the reversible hydrogen electrode as reference electrode. For RRDE measurements, two Solartron 1287 potentiostats were used to control disk and ring potentials, respectively, and an AFMRX rotator (Pine Instruments) was used for controlling the rotation speed. The electrochemical cell temperature was controlled at 25 °C using a water bath. Note that the *iR*-drop between the work electrode surface and the tip of the reference electrode may affect the data's accuracy [12]. To make the measurement more accurate, the *iR* drop was compensated using the function of the potentiostat during the measurements.

For electrode cleaning, the freshly prepared working electrode was immersed in N_2-saturated 0.5 M H_2SO_4 solution and electrochemically cleaned by repeatedly cycling the potential between 0.03 and 1.4 V vs. RHE for more than 20 cycles at a scan rate of 50 mV s^{-1}. The surface cyclic voltammetry (CV) was recorded with a potential scan rate of 50 mV s^{-1} between 0.05 and 1.2 V vs. RHE. The ORR measurements were performed by linear scan voltammetry between 0.05 and 1.0 V vs. RHE at 5 mV s^{-1} in 0.5 M O_2-saturated H_2SO_4 solution. For RRDE measurements, the potential of the Pt ring electrode was kept at 1.2 V vs. RHE where the oxidation of hydrogen peroxide was supposed to be under pure diffusion control.

3. Results and discussion

3.1. ORR behavior on Pt/C nanoparticle surfaces observed by RRDE

Fig. 1a shows the current–potential curves at different electrode rotation rates in O_2-saturated acid solution, recorded on a Pt/C coated glassy carbon disk electrode. The corresponding ring currents of catalyzed oxygen reduction reaction are shown in Fig. 1b. The disk current is the sum of two currents, one is the electron-transfer kinetic current, and the other is the diffusion current. From Fig. 1a, in the potential range approximately of 1.0–0.85 V vs. RHE, all currents do not change with increasing rotation rate, suggesting that the currents in this potential range are dominated by electron-transfer kinetics, while in the potential range of 0.60–0.05 V, the currents are a function of rotation rate and display well-defined limiting currents (or plateau currents), indicating the currents are controlled by the rate of O_2 diffusion from the bulk solution to the electrode catalyst surface. In the

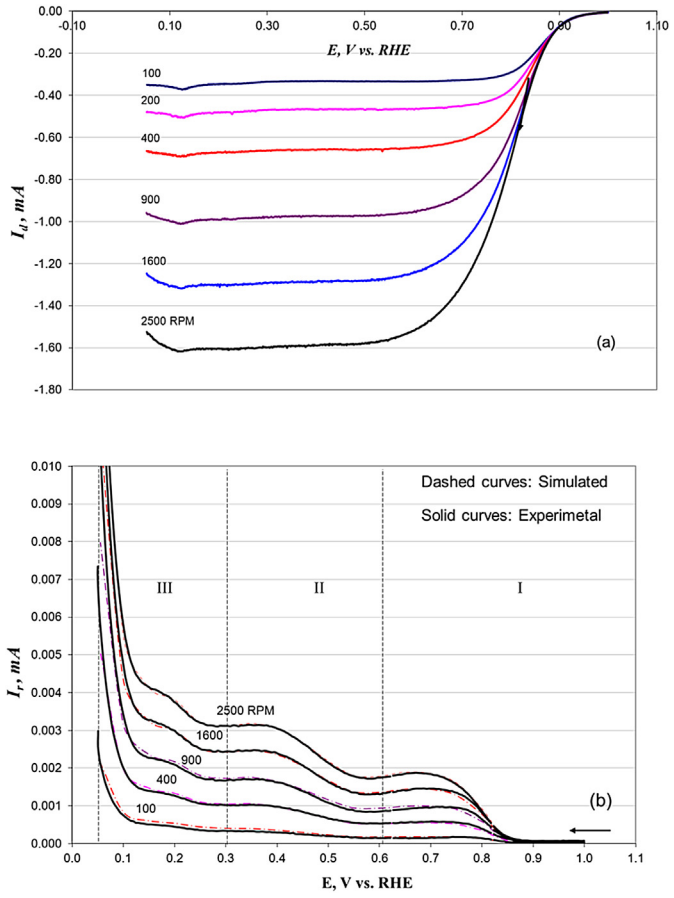

Fig. 1. (a) Current–potential curves of a glassy carbon electrode (0.25 cm^2) coated by Pt/C catalyst with a Pt loading of 48 mg cm^{-2}, recorded at different rotation rates in O_2 saturated 0.5 M H_2SO_4 aqueous solution with a potential scan rate of 5 mV s^{-1}; (b) Ring currents of the RRDE as a function of disk electrode potential at different rotation rates, recorded on a Pt ring electrode with a fixed potential of 1.2 V vs. RHE. The collection efficiency of the RRDE employed is 0.37.

potential range between 0.85 and 0.60 V, the currents are contributed by a mixed O_2 diffusion and electron-transfer kinetic process.

From the ring currents in Fig. 1b, it can be seen that there are mainly three regions on the curves as marked on the figure. This result was also observed on Pt/C particle surfaces in both acid and alkaline solutions [13–15]. The ring currents arise from the oxidation of hydrogen peroxide as an ORR by-product from the disk electrode, which is thrown onto the Pt-ring electrode where it is oxidized to form water. The three ring current curve regions, namely I, II, and III, may indicate that the ORR behavior on the disk electrode surface is different, or in other words, different current stages may reflect differences in Pt surface structure. In order to confirm this, Fig. 2 shows the surface cyclic voltammogram of a Pt/C surface measured in N_2-saturated solution, where three Pt-surfaces can be roughly divided into different potential ranges, which shows a consistency with the corresponding ring current stages shown in Fig. 1b.

Fig. 2 shows that Region I is located in the potential range of positive 0.60 V, which corresponds to a Pt surface covered by PtO_X (dominated by PtO); Region II is in the range of 0.30–0.60 V, which is the surface dominated by pure Pt; and Region III is in the potential range of 0.05–0.30 V, which mainly corresponds to the hydrogen-adsorbed Pt surfaces [16]. These assignments are also summarized in Table 1.

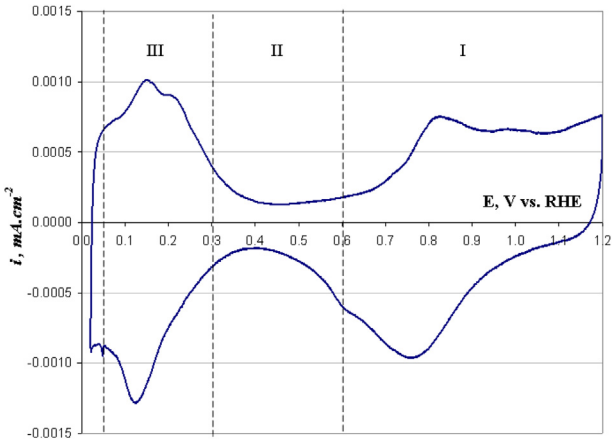

Fig. 2. Cyclic voltammogram of a glassy carbon electrode (0.25 cm^2) coated by Pt/C catalyst with a Pt loading of 48 mg cm^{-2}, recorded in O_2 saturated 0.5 M H_2SO_4 aqueous solution with a potential scan rate of 50 mV s^{-1}.

3.2. Model analysis for both 4-electron and 2-electron transfer process in the catalyzed ORR

The ring currents in Fig. 1b give a clear indication that for the Pt/C catalyzed ORR, besides the 4-electron transfer pathway from O_2 to H_2O, there is also a 2-electron transfer pathway from O_2 to H_2O_2. However, Fig. 1 shows that the disk current magnitudes are much higher than those of the ring current, for example, the ratios between the disk currents and the ring currents are in the range of 4000–400 in the potential range shown, indicating that the amount of H_2O_2 produced during the ORR on disk electrode should be insignificant. This suggests that the ORR on Pt/C nanoparticles is a mainly 4-electron transfer process from O_2 directly to H_2O.

Fig. 1b indicates that the ORR behavior in the three marked potential ranges is different. This may be because the status of the Pt particles surface is different in these three potential ranges, as listed in Table 1. In understanding the difference in ORR activity and the corresponding mechanism for these three surfaces, the method developed by Bocris' group for RRDE data analysis [2–4] can be employed to analyze the ORR mechanism and obtain the kinetic constants for different Pt surfaces. Note that the method initiated by Bocris' group has been validated and modified by many other groups in the literature [5–11]. The model is based on the RRDE measurements, where both ORR disk and ring currents and the electrode rotation rate are the key measurable variables. The hydrogen peroxide produced during ORR at the rotating disk electrode in a given potential can be carried by forced convection to the ring electrode where it will be oxidized at a high ring potential [17,18]. By referring to the literature and assuming that all H_2O_2 which is transported to the ring surface will be oxidized immediately, the ORR process on a Pt/C particle surface can be proposed as follows [8,17]:

In Fig. 3, all steps can be expressed by the following reaction equations:

$$O_2(\text{bulk}) \xrightarrow{\text{diffusio-convection},\ 0.201 D_{O_2}^{2/3} \nu^{-1/6}} O_2(\text{disk surface}) \qquad \text{(I)}$$

Table 1
Possible assignment for Pt-related surfaces at different potential ranges based on the cyclic voltammogram shown in Fig. 2.

Region	I	II	III
Electrode potential range (V vs. RHE)	>0.60	0.30–0.60	0.05–0.30
Pt surface status	PtO_X/Pt	Pt	Pt–H

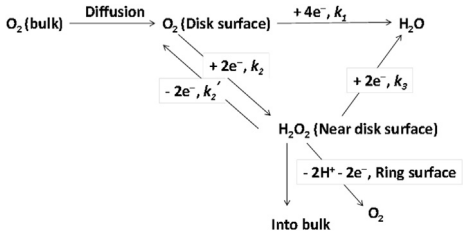

Fig. 3. Schematic of the oxygen reduction reaction (ORR) processes on a RRDE.

$$O_2(\text{disk surface}) + 4e^- + 4H^+ \xrightarrow{k_1} 2H_2O(\text{surface}) \quad \text{(II)}$$

$$O_2(\text{disk surface}) + 2e^- + 2H^+ \xrightarrow{k_2} H_2O_2(\text{disk surface}) \quad \text{(III)}$$

$$H_2O_2(\text{disk surface}) \xrightarrow{k_2'} O_2 + 2e^- + 2H^+(\text{disk surface}) \quad \text{(IV)}$$

$$H_2O_2(\text{disk surface})) + 2e^- + 2H^+ \xrightarrow{k_3} 2H_2O(\text{disk surface}) \quad \text{(V)}$$

$$H_2O_2(\text{disk surface}) \xrightarrow{\text{Convected to bulk solution and ring surface, } 0.201D_{H_2O_2}^{2/3}\nu^{-1/6}} xH_2O_2(\textit{ring surface}) + (1-x)H_2O_2(\text{bulk}) \quad \text{(VI)}$$

$$xH_2O_2(\text{ring surface}) \xrightarrow[\text{at high ring potential}]{\text{completed reaction}} x\left(O_2(\text{bulk}) + 2e^- + 2H^+\right) \quad \text{(VII)}$$

Reaction (I) is the diffusion–convection of the bulk O_2 onto the disk electrode surface with a rate constant of $0.201D_{O_2}^{2/3}\nu^{-1/6}$ (D_{O_2} is the diffusion coefficient of O_2, and ν is the kinematic viscosity of the electrolyte solution) cording to the RDE theory [18]; Reaction (II) is the direct 4-electron transfer and reduction of surface O_2 to produce H_2O with a reaction constant of k_1; Reaction (III) is a parallel 2-electron transfer reduction of O_2 to produce surface H_2O_2 with a reaction constant of k_2; Reaction (IV) is a 2-electron transfer oxidation of surface H_2O_2 to produce surface O_2 with a reaction constant of k_2'; Reaction (V) is a 2-electron transfer reduction of surface H_2O_2 to produce H_2O with a reaction constant of k_3; Reaction (VI) is the diffusion–convection of the surface H_2O_2 with a rate constant of $0.201D_{H_2O_2}^{2/3}\nu^{-1/6}$ ($D_{H_2O_2}$ is the diffusion coefficient of H_2O_2), part of which will go to bulk solution, and the other part will get onto the ring electrode where it is completely oxidized at a high ring potential through Reaction (VII).

Note that the effect of adsorbed electrolyte anions (SO_4^{2-}) on the Pt surface in the entire potential range studied may make some contribution to the obtained reaction rate constants [19]. For simplification and not diluting the main focuses, we assume that its contribution can be counted into the rate constants. If all the reactions are at steady-state on the disk electrode and the proton concentration can be combined into the reaction constants, an O_2 mass balance can be expressed as Equation (1) [17]:

$$B_{O_2}\omega^{1/2}\left(C_{O_2}^o - C_{O_2}^s\right) + k_2'C_{H_2O_2}^s = (k_1+k_2)C_{O_2}^s \quad (1)$$

where $B_{O_2}(=0.201D_{O_2}^{2/3}\nu^{-1/6})$ is the diffusion rate constant of O_2, $C_{O_2}^o$ is the bulk solution concentration of O_2, $C_{O_2}^s$ is the surface concentration of O_2, and ω is the electrode rotation rate in RPM. For H_2O_2,

$$k_2C_{O_2}^s = B_{H_2O_2}\omega^{1/2}C_{H_2O_2}^s + k_2'C_{H_2O_2}^s + k_3C_{H_2O_2}^s \quad (2)$$

where $B_{H_2O_2}(=0.201D_{H_2O_2}^{2/3}\nu^{-1/6})$ is the diffusion rate constant of H_2O_2, $C_{H_2O_2}^s$ is the surface concentration of H_2O_2. Equation (2) can also be written as:

$$\frac{C_{O_2}^s}{C_{H_2O_2}^s} = \frac{B_{H_2O_2}\omega^{1/2} + k_2' + k_3}{k_2} \quad (3)$$

The total disk electrode current (I_d) can be expressed as:

$$I_d = 4F\pi r^2k_1C_{O_2}^s + 2F\pi r^2k_2C_{O_2}^s - 2F\pi r^2k_2'C_{H_2O_2}^s + 2F\pi r^2k_3C_{H_2O_2}^s \quad (4)$$

where r is the radius of the disk electrode (πr^2 is the area of the disk electrode). If at the beginning of the reaction, there is no H_2O_2 in the solution, the limiting current for H_2O_2 production ($I_{dl,\ H_2O_2}$) on disk electrode can be expressed as Equation (5):

$$I_{dl,H_2O_2} = 2F\pi r^2B_{H_2O_2}\omega^{1/2}C_{H_2O_2}^s \quad (5)$$

According to the definition of collection efficiency (N), the current at the ring electrode (I_r) should be expressed as Equation (6):

$$I_r = I_{dl,H_2O_2}N = 2F\pi r^2B_{H_2O_2}\omega^{1/2}C_{H_2O_2}^sN \quad (6)$$

Combining Equations (3), (4) and (6), the following equation can be obtained:

$$\frac{I_d}{I_r} = \frac{1}{N}\left(1+\frac{2k_1}{k_2}\right) + \frac{1}{B_{H_2O_2}N}\left(\left(1+\frac{2k_1}{k_2}\right)(k_3+k_2') + k_3 - k_2'\right)\omega^{-1/2} \quad (7)$$

This is an important equation for obtaining reaction constants from the slope and intercept of the I_d/I_r vs. $\omega^{-1/2}$ experimental plot. Fig. 4 shows three representative plots of I_d/I_r vs. $\omega^{-1/2}$ at three electrode potentials located in the three regions shown in Fig. 2. It can be seen that all of them are straight lines with slopes and intercepts from which the values of $1 + 2k_1/k_2$ and $((1+2k_1/k_2)(k_3+k_2')+k_3-k_2')$ can be estimated at different potentials.

However, based on Equation (7), we can only obtain the values of k_1/k_2, the individual value of k_1, k_2, k_2' or k_3, and in particular the values of k_1 and k_2, can't be obtained. As discussed below, the individual values of $k_2'$and k_3 can be obtained using another form of Equation (7). This alternative equation of Equation (7) also allows the estimation of apparent or overall number of electron transfer in the ORR process, which is one of the most important parameters in ORR mechanism. To express the relationship among the apparent electron number (n), the disk current (I_d) and the ring current (I_r),

the ORR mechanism shown in Fig. 3 is used to obtain the expression of this parameter. Based on Equation (1), the disk current can be related to the apparent electron transfer number (n) by Equation (8):

$$I_d = nF\pi r^2\left(B_{O_2}\omega^{1/2}\left(C^o_{O_2} - C^s_{O_2}\right) + k_2^{'}C^s_{H_2O_2}\right)$$
$$= nF\pi r^2(k_1 + k_2)C^s_{O_2} \Rightarrow \frac{4}{n}I_d = 4F\pi r^2(k_1 + k_2)C^s_{O_2} \quad (8)$$

According to Fig. 3, the disk current can also be expressed as:

$$I_d = 4F\pi r^2 k_1 C^s_{O_2} + 2F\pi r^2 k_2 C^s_{O_2} - 2F\pi r^2 k'_2 C^s_{H_2O_2} + 2F\pi r^2 k_3 C^s_{H_2O_2} \quad (9)$$

and the limiting current at the ring electrode (I_r) can be expressed as:

$$I_r = 2F\pi r^2 B_{H_2O_2}\omega^{1/2}C^s_{H_2O_2}N \Rightarrow C^s_{H_2O_2} = \frac{I_r}{N}\frac{1}{2F\pi r^2 B_{H_2O_2}\omega^{1/2}} \quad (10)$$

Combining Equations (8)–(10), the following equation can be obtained:

$$\frac{4I_d}{n} = I_d + \frac{I_r(k'_2 - k_3)}{B_{H_2O_2}\omega^{1/2}N} + 2F\pi r^2 k_2 C^s_{O_2} \quad (11)$$

According to Equations (3) and (10), $C^s_{O_2}$ can be expressed as:

$$C^s_{O_2} = \frac{I_r}{N}\frac{1}{2F\pi r^2 B_{H_2O_2}\omega^{1/2}}\frac{B_{H_2O_2}\omega^{1/2} + k'_2 + k_3}{k_2} \quad (12)$$

Substituting Equation (12) into Equation (11), Equation (13) can be obtained:

$$\frac{I_d}{I_r} = \frac{1}{N}\left(\frac{n}{4-n}\right) + \frac{1}{N}\left(\frac{n}{4-n}\right)\frac{2k'_2}{B_{H_2O_2}}\omega^{-1/2} \quad (13)$$

The plot of I_d/I_r vs. $\omega^{-1/2}$ can give an intercept, $1/N(n/4-n)$, from which the apparent ORR electron transfer number can be obtained, and a slope, $1/N(n/4-n)2k'_2/B_{H_2O_2}$, from which the reaction constant of k'_2 can be obtained. Fig. 5 shows the representative plots of I_d/I_r vs. $\omega^{-1/2}$ at three electrode potentials.

In particular, Equations (7) and (13) are equal to each other where $n/4-n = 1+2k_1/k_2$, and $k'_2(1+2k_1/k_2) = (1+2k_1/k_2)(k_3+k'_2)+k_3-k'_2$. Based on this relationship, the following Equations can be obtained:

$$n = \frac{2\left(1+\frac{2k_1}{k_2}\right)}{1+\frac{k_1}{k_2}} = \frac{2(2k_1+k_2)}{k_1+k_2} \quad (14)$$

$$k_3 = \frac{k'_2}{\left(1+\frac{k_1}{k_2}\right)} \quad (15)$$

From the intercepts of I_d/I_r vs. $\omega^{-1/2}$plots, the value of k_1/k_2 at different electrode potentials can be calculated using Equation (7), then the apparent ORR electron transfer numbers (n) can be calculated using Equation (14). From the slopes of Equation (13), the values of k'_2at different potentials can be obtained, from which the values of k_3 can be calculated using Equation (15). Fig. 5 shows the values of k'_2 and k_3 as a function of potential. It can be seen that both values are not sensitive to the Pt surface state. However, both of them are sensitive to the electrode potential.

Until now, we have obtained the values of k_1/k_2, k'_2 and k_3. In order to obtain the individual values of k_1 and k_2, an additional equation has to be explored. The theoretical ORR limiting current (I_{dl,O_2}) at the disk electrode can be used to obtain a new equation:

$$I^T_{dl,O_2} = 4F\pi r^2 B_{O_2}\omega^{1/2}C^o_{O_2} \quad (16)$$

Combining Equations (1) and (16), Equation (17) can be obtained:

$$I^T_{dl,O_2} = 4F\pi r^2\left(\left(k_1 + k_2 + B_{O_2}\omega^{1/2}\right)C^s_{O_2} - k'_2 C^s_{H_2O_2}\right) \quad (17)$$

Combining Equations (4), (6) and (16), Equation (18) can be obtained:

$$\frac{I^T_{dl,O_2} - I_d}{I_r} = \frac{1}{N}\left(1 + \frac{2(k_3+k'_2)}{k_2}\frac{B_{O_2}}{B_{H_2O_2}}\right) + \frac{2B_{O_2}}{k_2 N}\omega^{1/2} \quad (18)$$

The plot of $I^T_{dl,O_2} - I_d/I_r$ vs. $\omega^{1/2}$ will give a slope of $2B_{O_2}/k_2N$, from which, k_2 can be obtained. Unfortunately, if k_2 is larger than $2B_{O_2}/N$in Equation (18), $2B_{O_2}/k_2N$ will be less than 1, the plot of $I^T_{dl,O_2} - I_d/I_r$ vs. $\omega^{1/2}$ will not be sensitive to $\omega^{1/2}$, the error in the value of $2B_{O_2}/k_2N$ obtained may be too large for it to be used. This was confirmed using the data in Fig. 1. Therefore, we have to find

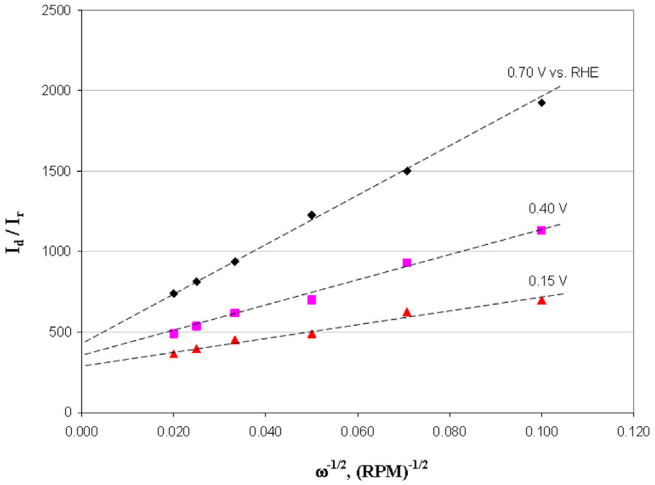

Fig. 4. Plots of I_d/I_r vs. $\omega^{-1/2}$ at three electrode potentials in the three regions as indicated in Fig. 2, with data from Fig. 1.

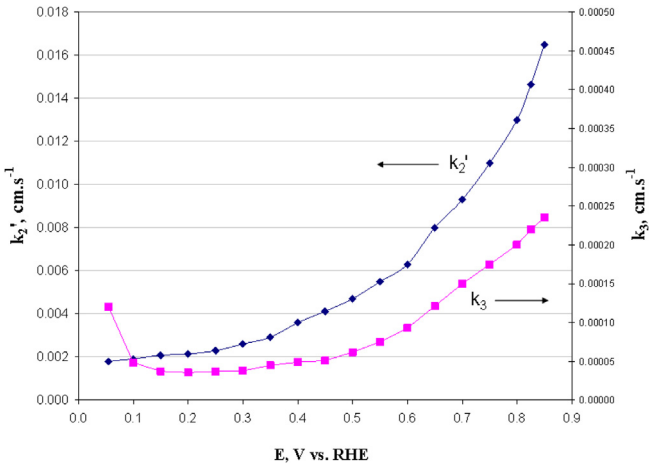

Fig. 5. Reaction constants of k'_2 and k_3 as a function of electrode potential, simulated using Equations (7) and (13) based on the data in Fig. 1.

another way to separate out the value of either k_1 or $k_2$from the value of k_1/k_2. In this case, Koutecky–Levich theory may be used.

According to Koutecky–Levich theory, the RDE disk current (I_{dl,O_2}) can be expressed as:

$$\frac{1}{I_d} = \frac{1}{I_k} + \frac{1}{I_{dl,O_2}} \Rightarrow I_k = \frac{I_d I_{dl,O_2}}{I_{dl,O_2} - I_d} \tag{19}$$

where I_k is the kinetic current, and I_{dl,O_2} is the limiting current, respectively. According to Equation (1), I_d and I_{dl,O_2} can be expressed as Equations (20) and (21), respectively:

$$I_d = nF\pi r^2 (k_1 + k_2) C^s_{O_2} \tag{20}$$

$$I_{dl,O_2} = nF\pi r^2 B_{O_2} \omega^{1/2} C^o_{O_2} \tag{21}$$

Substituting both Equations (20) and (21) into Equation (19), the kinetic current can be expressed as:

$$I_k = nF\pi r^2 \frac{B_{O_2}\omega^{1/2}(k_1 + k_2) C^s_{O_2} C^o_{O_2}}{B_{O_2}\omega^{1/2} C^o_{O_2} - (k_1 + k_2) C^s_{O_2}} \tag{22}$$

According to Equations (1) and (2), the surface concentration of O_2 can be expressed as:

$$C^s_{O_2} = \frac{B_{O_2}\omega^{1/2} C^o_{O2}}{k_1 + k_2 + B_{O_2}\omega^{1/2} - k'_2 k_2 / (B_{H_2O_2}\omega^{1/2} + k'_2 + k_3)} \tag{23}$$

Substituting Equation (23) into Equation (22), Equation (24) can be obtained:

$$I_k = nF\pi r^2 C^o_{O_2} \frac{B_{O_2}\omega^{1/2}(B_{H_2O_2}\omega^{1/2} + k'_2 + k_3)(k_1 + k_2)}{B_{O_2}\omega^{1/2}(B_{H_2O_2}\omega^{1/2} + k'_2 + k_3) - k'_2 k_2} \tag{24}$$

When the electrode rotation rate is very large, such as, $\omega \to \infty$(or $\omega^{-1/2} \to 0$), the kinetic current will become the pure electron transfer controlled current:

$$I_k = nF\pi r^2 (k_1 + k_2) C^o_{O_2} = nF\pi r^2 \left(\frac{k_1}{k_2} + 1\right) k_2 C^o_{O_2} \tag{25}$$

Substituting Equation (25) into Equation (19), Koutecky–Levich equation can be obtained:

$$\frac{1}{I_d} = \frac{1}{I_k} + \frac{1}{I_{dl,O_2}} = \frac{1}{nF\pi r^2 \left(\frac{k_1}{k_2} + 1\right) k_2 C^o_{O_2}} + \frac{1}{nF\pi r^2 B_{O_2} C^o_{O_2}} \omega^{-1/2} \tag{26}$$

The plot of $1/I_d$ vs. $\omega^{-1/2}$ using the data shown in Fig. 1 can give a straight line, where from the intercept (when $\omega^{-1/2} = 0$), the value of $(k_1/k_2 + 1)k_2$ can be obtained. Since the value of k_1/k_2 is known from Equation (7), individual values of k_1 and k_2 can be resolved. Based on the data shown in Figs. 1 and 6a shows three representative plots of $1/I_d$ vs. $\omega^{-1/2}$ at three potentials located at the three regions in Fig. 2. Fig. 6b shows k_1 and k_2 obtained as a function of electrode potential. It can be seen that both k_1 and k_2 are sensitive to the status of the Pt/C particle surface, which will be further discussed in a later section.

Note that in the potential range less than 0.5 V in Fig. 6b, the values of both k_1 and k_2 obtained using Koutecky–Levich plot were found to have standard errors as high as 18%. The values shown in Fig. 6b are the average results of 5 sets of measurements. However, the values in the potential range higher than 0.5 V had only ~3% of error.

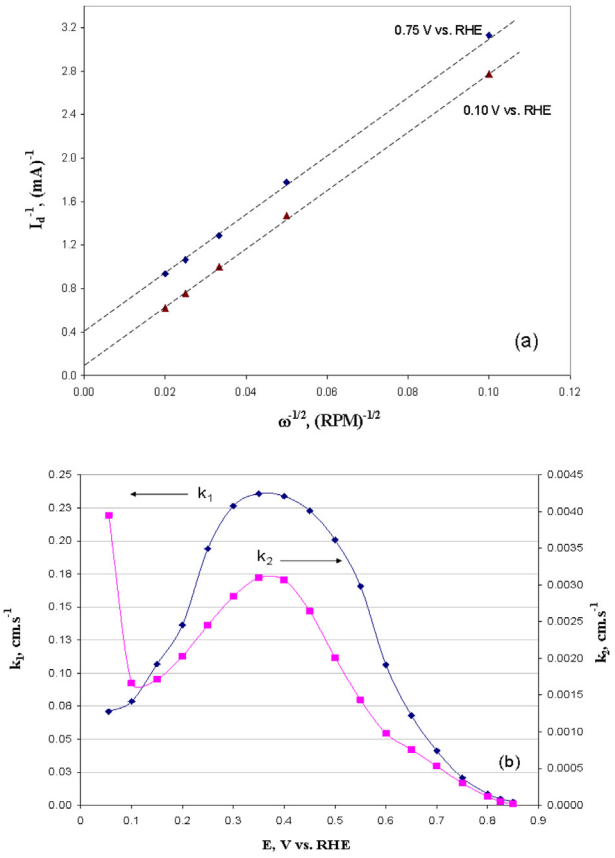

Fig. 6. (a) plots of $1/I_d$ vs. $\omega^{-1/2}$ at two electrode potentials, obtained based on the data in Fig. 1 using Equation (26); (b) values of and as a function of electrode potential.

3.3. Apparent ORR electron transfer number and percentage H_2O_2 produced during the ORR

As discussed above, the apparent ORR electron transfer number can be obtained using Equation (13) based on the experimental RRDE data. Equation (3) can be rearranged as Equation (27):

$$n = \frac{4I_d N}{I_d N + I_r \left(1 + \frac{2k'_2}{B_{H_2O_2}} \omega^{-1/2}\right)} \tag{27}$$

According to Equation (7), apparent ORR electron transfer numbers can be calculated in the potential range studied, as shown in Fig. 7. It can be seen that the apparent electron transfer numbers are in the range of 3.95–3.99, except the one obtained at 0.055 V, which indicates the ORR on Pt/C surfaces is dominated by a 4-electron transfer process reducing O_2 directly to H_2O.

Note that if there is no reaction of H_2O_2 to O_2 in Fig. 3, that is $k'_2 = 0$, Equation (27) will become Equation (28):

$$n = \frac{4I_d N}{I_d N + I_r} \tag{28}$$

This is the equation normally used in literature. Apparently, this equation is only valid when Reaction (IV) from H_2O_2 to O_2 in Fig. 3 does not exist ($k'_2 = 0$). This equation indicates that when the ORR is a total 4-electron transfer process, $I_r = 0$ the apparent number is 4, and when the ORR is a pure 2-electron transfer process, $I_r = I_d N$, Equation (28) will give an apparent number of 2.

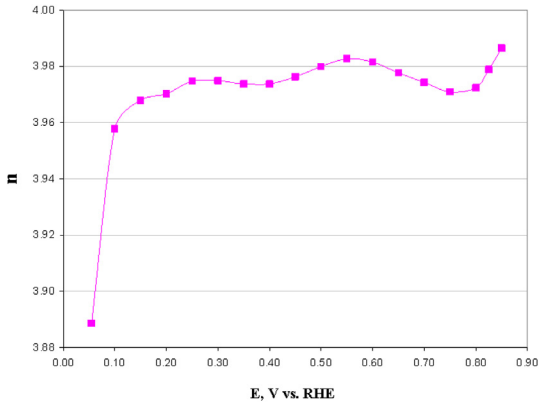

Fig. 7. Apparent ORR electron transfer numbers at the potential range studied. Simulated based on the data in Fig. 1 using Equation (13).

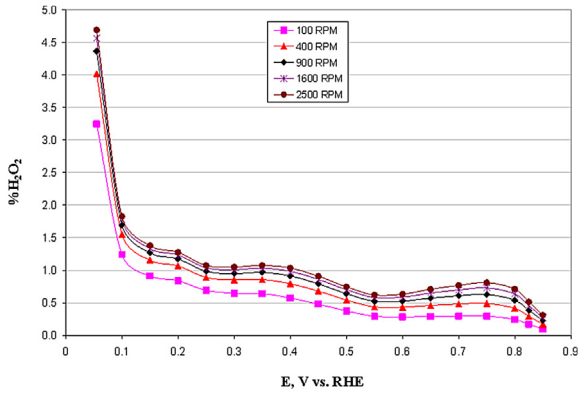

Fig. 8. Percentage of H_2O_2 produced during the ORR as a function of electrode potential at different electrode rotation rates. Simulated based on Data from Fig. 1 and Equation (30).

Regarding the percentage of H_2O_2 produced from the ORR (%H_2O_2), the mass flows can be used for calculation according to Fig. 3:

$$\begin{aligned}\%H_2O_2 &= 100\frac{\text{Total moles of } H_2O_2 \text{ produced}}{\text{Total moles of } O_2 \text{ reacted}}\\ &= 100\frac{k_2C^s_{O_2} - k_3C^s_{H_2O_2} - k'_2C^s_{H_2O_2}}{k_1C^s_{O_2} + k_2C^s_{O_2}}\\ &= \frac{2F\pi r^2k_2C^s_{O_2} - 2F\pi r^2k_3C^s_{H_2O_2} - 2F\pi r^2k'_2C^s_{H_2O_2}}{\frac{2}{n}\left(nF\pi r^2k_1C^s_{O_2} + nF\pi r^2k_2C^s_{O_2}\right)}\end{aligned} \quad (29)$$

Combining Equations (10) and (12), Equation (29) can be obtained:

$$\%H_2O_2 = 50(4-n)\frac{B_{H_2O_2}}{B_{H_2O_2} + k'_2\omega^{-1/2}} \quad (30)$$

In Equation (30), the values of n, $B_{H_2O_2}$, k'_2 and ω are known, the values of %H_2O_2 can be calculated, as shown in Fig. 8 for the whole potential range at different electrode rotation rates. It can be seen that the percentage of H_2O_2 during the ORR is less than 2% except for that at the potential of 0.055 V. The percentage of H_2O_2 is increased with increasing electrode rotation rate. Qualitatively, this is because at higher rotation rates, the H_2O_2 produced at the disk electrode can be quickly thrown out before it has enough time to be consumed through reaction paths k'_2 and k_3 shown in Fig. 3.

From Equation (30), it can be seen that if $k'_2 = 0$, Equation (30) will become:

$$\%H_2O_2 = 50(4-n) \quad (31)$$

Note that this Equation (31) is the equation normally used for calculating %H_2O_2, which is only applicable to the case where there is no reaction of H_2O_2 to O_2 in Fig. 3.

3.3. Discussion about ORR reaction constants at the corresponding Pt/C surfaces

To validate these values of k_1, k_2, $k'_2$and k_3 shown in Figs. 5 and 6, the ring current simulation using these values was carried out, and the simulated ring currents were plotted as a function of disk potential at different electrode rotation rates, as shown by the dashed curves in Fig. 1a. It can be seen that the simulated curves are fairly close to those measured experimentally with less than ±5% error, indicating that the obtained values of k_1, k_2, $k'_2$and k_3 should be correct.

Normally, for comparing catalyst activity, a specific activity, that is the activity per unit weight of the catalyst, makes more sense. To do so, all values of k_1, k_2, k'_2 and k_3 were divided by the catalyst content in the catalyst layer (0.048 mgPt cm^{-2} in this work), and the specific reaction constants are expressed as k_{1s}, k_{2s}, k'_{2s}, and k_{3s}, respectively.

For the convenience of discussion, all normalized reaction constants were plotted together and are shown in Fig. 9 for comparison. From Fig 9, it can be seen that all values of k_{1s}, k_{2s}, k'_{2s}, and k_{3s} are strongly dependent on electrode potential. There are significant differences in curve trends. For example, for Reactions (II) and (III) of the ORR, the reaction constants, k_{1s} and k_{2s}, are both sensitive to the electrode surface state, while for Reactions (IV) and (V), neither reaction constant k'_{2s}, nor k_{3s}, are sensitive to the electrode surface state although they are strongly dependent on the electrode potential. In the following section, we will give a further discussion on the sensitivities of these constants to the Pt surface state.

3.3.1. PtO_X covered Pt surface (>0.6 V vs. RHE)

PtO_X covered Pt surface is roughly located in the potential range of >0.6 V vs. RHE, as shown in Fig. 2. In this potential range, the ORR constants, k_{1s} and k_{2s}, are both monotonically increasing with reducing electrode potential, as seen in Fig. 9. This probably reflects

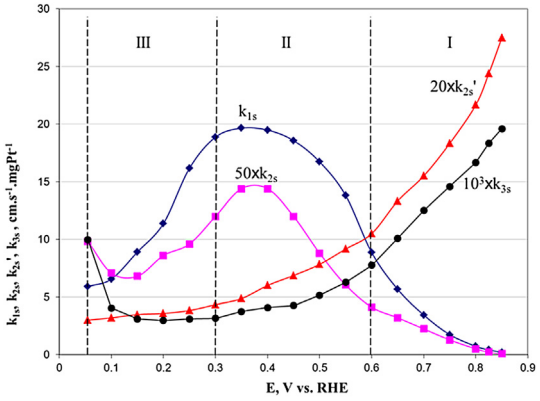

Fig. 9. ORR specific reaction constants (k_{1s}, k_{2s},k'_{2s} and k_{3s}) as a function of electrode potentials, recorded on a Pt/C-based catalyst layer coated glassy carbon electrode in O_2 saturated 0.5 M H_2SO_4 solution, simulated using Equations (7), (13) and (18) based on RRDE data shown in Fig. 1. Constants used for these calculations are: $D_{O_2} = 1.9 \times 10^{-5}$ cm^2 s^{-1}; $D_{H_2O_2} = 1.7 \times 10^{-5}$ cm^2 s^{-1}; $\nu = 0.01$ cm^2 s^{-1}, $N = 0.37$.

the difference in ORR activities of the PtO_X and Pt surfaces, that is, the ORR activity of PtO_X is much lower than that of pure Pt surface, which has been proven using fuel cell tests [20]. With reducing electrode potential, the coverage of clean Pt surface would increase due to the reduction of PtO_x to Pt, resulting in a higher ORR activity or higher reaction constant.

Normally, the dependence of reaction constants on potential can be treated using Butler–Volmer theory if the electrode surface state is constant under changing potential. Then, the kinetic current (I_{k_i}) of ORR can be expressed as Equation (32)

$$I_{k_i} = n_i F A k_i C_{O_2}^o = nFAk_i C_{O_2}^o \exp\left(-\frac{\alpha_i n_{\alpha_i} F\left(E - E_{O_2}^o\right)}{RT}\right)$$
$$\Rightarrow k_i = k_i^o \exp\left(-\frac{\alpha_i n_{\alpha_i} F\left(E - E_{O_2}^o\right)}{RT}\right) \quad (32)$$
$$\Rightarrow E = E_{O_2}^o + \frac{2.303RT}{\alpha_i n_{\alpha_i} F}\log\left(k_i^o\right) - \frac{2.303RT}{\alpha_i n_{\alpha_i} F}\log(k_i)$$

where k_i^o is the reaction constant at the equilibrium potential ($E_{O_2}^o$ at standard conditions), α_i and n_{α_i} are the electron transfer coefficients and number in the reaction rate determining step, respectively. The plot of E vs. $\log(k_i)$, called the Tafel plot, gives a slope ($2.303RT/\alpha_i n_{\alpha_i} F$), and intercept ($E_{O_2}^o + 2.303RT/\alpha n_\alpha F \log(k_i^o)$), from which both the kinetic parameters of $\alpha_i n_{\alpha_i}$ and k_i^o can be calculated. Fig. 10 shows the plots of E vs. $\log(k_{1s})$ and $\log(k_{2s})$. It can be seen that both of the curves are not the straight lines predicted by the Tafel Equation (32). This is because the status of the electrode surface is changing with changing electrode potential, leading to the observed deviation from the theoretical prediction. In the literature, there are two slopes for E vs. $\log(k_i)$ plots which can be observed [15]. In Fig. 10, two sets of arbitrary slope/intercept can also be seen, where one is in the potential range of 0.75–0.85 V, and the other is in the potential range of 0.60–0.75 V. We believe that further treatment using these two set of slopes/intercepts to obtain kinetic parameters such as $\alpha_i n_{\alpha_i}$ and k_i^o may not be appropriate because the ORR process is proceeding on an electrode surface that is not constant with changing potential.

Regarding k'_{2s} and k_3 in this potential range of >0.6 V, both of their values are monotonically increasing with increasing electrode potential. The increase in the value of k'_{2s}, is understandable because Reaction (IV) is an electro-oxidation reaction, whose reaction constant should be increasing with increasing electrode potential. However, it is difficult to understand why the value of k_3 is also increasing with increasing electrode potential, which is not predicted for an electro-reduction such as Reaction (V). Further model modification may be needed for understanding this behavior.

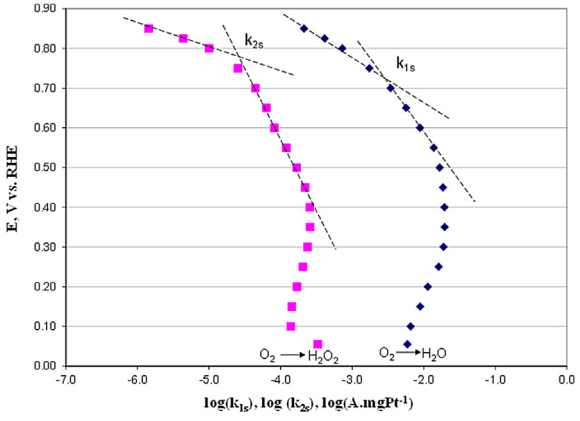

Fig. 10. Tafel plots for oxygen reduction reactions of O_2 to H_2O and O_2 to H_2O_2. Both data sets are from Fig. 9 for k_{1s} and k_{2s} in the potential range of positive 0.6 V vs. RHE.

3.3.2. Pure Pt surface (0.3–0.6 V vs. RHE)

From Fig. 2, it can be seen that the potential range of 0.3–0.6 V is roughly corresponding to the pure Pt dominated surface status. As shown in Fig. 9, in this potential range, both the values of k_1 and k_2 reach their maximum, demonstrating that the pure Pt surface has a superior ORR activity than that of PtO_X covered Pt surface.

3.3.3. Hydrogen adsorbed Pt surface (<0.3 V vs. RHE)

Fig. 9 shows that after both k_1 and k_2 reach their maximum at 0.4 V, they start to decrease with a further decrease in electrode potential. From Fig. 2, it can be seen that in the potential range of <0.3 V, the Pt surface is covered with hydrogen to form a Pt–H surface. For an inner sphere ORR mechanism, the formation of the Pt–O_2 adducts is the first step. In the presence of O_2, there would be a competition between H and O_2 for the Pt sites ($H^+ + e^- + Pt \rightarrow Pt - H$ and $O_2 + Pt \rightarrow Pt - O_2$). The bond energy for $Pt - H$ is much higher than that for $Pt - O_2$, thus the ORR may happen on the available Pt sites. With decreasing electrode potential, the $Pt - H$ coverage will increase, and the available number of Pt sites for the formation of Pt–O_2 adduct will decrease so that the ORR process on such a limited Pt surface should be slower than that on a pure or clean Pt surface. This may qualitatively explain why the ORR constants decrease with decreasing electrode potential.

4. Conclusion

The ORR on a Pt/C-based thin catalyst layer was recorded using RRDE technique in an O_2-saturated acid solution; and the disk and ring currents obtained as well as the rotation rates were analyzed using a modified model for obtaining the reaction constants in different electrode potential ranges. The reaction constants obtained were also validated using the experimental disk and ring currents. To account for the effect of Pt loading on the ORR constants, mass specific reaction constants were also defined in this paper.

In the potential range of 0.05–0.85 V, the surface cyclic voltammograms recorded using the same Pt/C-based catalyst layer in a N_2-saturated acidic solution were used to identify the Pt surface state. There were three potential ranges, < 0.30, 0.30–0.60, and >0.60 V vs. RHE, which correspond to three Pt surface states: hydrogen-adsorbed Pt surface (Pt–H); pure Pt surface (Pt); and Pt oxide covered Pt surface (PtO_X/Pt), respectively. Based on the experimental data, the results calculated from the proposed model and Koutecky–Levich plots revealed that the ORR constants on these three different Pt surfaces were significantly different. Compared to Pt–H and PtO_X/Pt surfaces, the most active surface for promoting the ORR was the pure or clean Pt surface. The modified model could also give formulas for calculating the apparent ORR electron transfer number (n) and the percentage of H_2O_2 produced during the ORR process (%H_2O_2). These formulas indicated that the commonly used formulas for calculating n and %H_2O_2 have some limitations.

Acknowledgments

The authors wish to thank the National Research Council of Canada (NRC) for the support of this work. Dr. Francois Girard and Mr. Ryan Baker's proof reading are highly appreciated.

References

[1] Chapter 2, Electrocatalytic Oxygen Reduction Reaction C. Song, J.J. Zhang, PEM Fuel Cell Electrocatalysts and Catalyst Layer – Fundamentals and Applications, Springer, London, 2008.
[2] A. Damjanovic, M.A. Genshaw, J.O.'M. Bocris, J. Phys. Chem. 70 (11) (1966) 3761–3762.
[3] M.A. Genshaw, A. Damjanovic, J.O.'M. Bocris, J. Phys. Chem. 71 (12) (1967) 3722–3731.
[4] A. Damjanovic, M.A. Genshaw, J.O.'M. Bocris, J. Electrochem. Soc. 114 (5) (1967) 466–472.
[5] H.S. Wroblowa, Y.C. Pan, G. Razumney, J. Electroanal. Chem. 69 (1976) 195–201.
[6] J.C. Huang, R.K. Sen, E. Yeager, J. Electrochem. Soc. 126 (1979) 786–792.
[7] W.E. O'Grady, E.J. Taylor, S. Srinivasan, J. Electroanal. Chem. 132 (1982) 137–150.
[8] K.L. Hsueh, D.T. Chin, S. Srinivasan, J. Electroanal. Chem. 153 (1983) 79–95.
[9] N.A. Anastasljevic, V. Vesovic, R.R. Adzic, J. Electroanal. Chem. 228 (1987) 305–316.
[10] N.A. Anastasljevic, V. Vesovic, R.R. Adzic, J. Electroanal. Chem. 229 (1987) 317–325.
[11] N.A. Anastasljevic, V. Vesovic, R.R. Adzic, J. Electroanal. Chem. 218 (1987) 53–63.
[12] D. Van der Cilet, D.S. Strmcnik, C. Wang, V.R. Stamenkovic, N.M. Markovic, M.T.M. Koper, J. Electroanal. Chem. 647 (2010) 29–34.
[13] O. Antoine, R. Durand, J. Appl. Electrochem. 30 (2000) 839–844.
[14] N. Ramaswamy, S. Mukerjee, Adv. Phys. Chem. 2012 (2012) 1–17. Article ID: 491604.
[15] U.A. Paulus, T.J. Schmit, H.S. Gasteiger, R.J. Behm, J. Electroanal. Chem. 495 (2001) 134–145.
[16] N.M. Markovic, H.A. Gasteiger, P.N. Ross Jr., J. Phys. Chem. 99 (11) (1995) 3411–3415.
[17] Q.X. Cha, An Introduction to Electrode Kinetics, Chinese Science Press, Beijing, 2005.
[18] Allen J. Bard, Larry F. Faulkner, Electrochemical Methods–Fundamentals and Applications, Wiley, New York, 2001.
[19] N.M. Markovic, T.J. Schmidt, V. Stamenkovic, P.N. Ross, Fuel Cells 1 (2) (2001) 105–116.
[20] C. Song, Y. Tang, J.L. Zhang, J. Zhang, H. Wang, J. Shen, S. McDermid, J. Li, P. Kozak, Electrochim. Acta 52 (7) (2007) 2552–2561.